

Surface depletion field in 2D perovskite microplates: Structural phase transition, quantum confinement and Stark effect

Wancai Li¹, Chen Fang¹, Haizhen Wang², Shuai Wang¹, Junze Li¹, Jiaqi Ma¹, Jun Wang¹, Hongmei Luo² (), and Dehui Li¹ ()

Received: 21 July 2019 / Revised: 19 September 2019 / Accepted: 21 September 2019

ABSTRACT

Surface depletion field would introduce the depletion region near surface and thus could significantly alter the optical, electronic and optoelectronic properties of the materials, especially low-dimensional materials. Two-dimensional (2D) organic–inorganic hybrid perovskites with van der Waals bonds in the out-of-plane direction are expected to have less influence from the surface depletion field; nevertheless, studies on this remain elusive. Here we report on how the surface depletion field affects the structural phase transition, quantum confinement and Stark effect in 2D (BA)₂Pbl₄ perovskite microplates by the thickness-, temperature- and power-dependent photoluminescence (PL) spectroscopy. Power dependent PL studies suggest that high-temperature phase (HTP) and low-temperature phase (LTP) can coexist in a wider temperature range depending on the thickness of the 2D perovskite microplates. With the decrease of the microplate thickness, the structural phase transition temperature first gradually decreases and then increases below 25 nm, in striking contrast to the conventional size dependent structural phase transition. Based on the thickness evolution of the emission peaks for both high-temperature phase and low-temperature phase, the anomalous size dependent phase transition could probably be ascribed to the surface depletion field and the surface energy difference between polymorphs. This explanation was further supported by the temperature dependent PL studies of the suspended microplates and encapsulated microplates with graphene and boron nitride flakes. Along with the thickness dependent phase transition, the emission energies of free excitons for both HTP and LTP with thickness can be ascribed to the surface depletion induced confinement and Stark effect.

KEYWORDS

two-dimensional (2D) perovskite, thickness, surface depletion field, structural phase transition, quantum confinement, Stark effect

1 Introduction

Materials with the same chemical compositions can exhibit dramatically different properties depending on how the atoms arrange, which was reflected by their dimensionality and crystal structure [1–3]. Reducing the dimensionality of materials would introduce quantum confinement effect leading to a series of novel properties that the macroscopic scale materials do not have, whereas the structural phase change can significantly alter the optical and electronic properties of the materials [4, 5]. In addition, the increase of the surface-to-volume ratio in low-dimensional materials could introduce strong surface depletion field, leading to the surface depletion induced quantum confinement and Stark effect.

Previous studies reveal that the structural phase transition strongly depends on the physical size of a material and generally the phase transition temperature would decrease with the shrinkage of the material size, which has been observed in many confined systems such as three-dimensional (3D) perovskites [6], nanocrystals and two-dimensional (2D) layered materials such as NbSe₂ [7, 8] and TaS₂ [9, 10]. To explain such size dependent structural phase transition, a number of competing theories have been developed including the lack of nucleation sites, internal pressure and surface energy difference between polymorphs for different material systems [6, 11, 12]. Therefore, it is of great relevance to explore the size dependent

structural phase transition in new material systems for both the fundamental investigations and the potential optoelectronic applications [13].

As an emerging material system, 2D Ruddlesden-Popper hybrid lead iodide perovskites exhibit a natural layered and quantum well structure, strong exciton binding energy and better environmental stability and thus have recently attracted growing attention [14, 15]. The general chemical formula of 2D perovskites can be expressed as R₂A_{n-1}M_nX_{3n+1}, where R is long chain molecular cation while A is organic cation, M and X are divalent metal and halide anion, respectively [16]. The integer n represents the layer number of inorganic layer sandwiched between two layers of organic cation A [17]. With such unique crystal structure, 2D perovskites equip the original optical properties of 2D inorganic layers while inheriting the flexibility and diversity of organic compositions compared with the traditional van der Waals materials [18-20]. While the bandgap of 2D perovskites can be readily tuned by changing the layer number n and chemical compositions, the extremely large exciton binding energy is present due to the dielectric confinement, which renders 2D perovskites be ideal candidates for polaritonic devices [21]. Furthermore, the weak van der Waals coupling among inorganic layers allow us to exfoliate thin flakes to integrate with other layered materials to extend their functionalities and to investigate their size dependent physical properties [6]. To this end, it is of great significance

¹ School of Optical and Electronic Information and Wuhan National Laboratory for Optoelectronics, Huazhong University of Science and Technology, Wuhan 430074, China

² Department of Chemical and Materials Engineering, New Mexico State University, Las Cruces, NM 88003, USA

[©] Tsinghua University Press and Springer-Verlag GmbH Germany, part of Springer Nature 2019

to study the surface depletion field induced effects in 2D perovskites, which would be of utmost relevance to the optical and electronic properties of the 2D perovskites [4, 10, 22-25]. Nevertheless, studies on those aspects still remain elusive in 2D perovskites.

Here we report on how the surface depletion field affects the structural phase transition, quantum confinement and Stark effect in 2D (BA)₂PbI₄ (donated as BAPI, BA = C₄H₉NH₃) perovskite microplates by the thickness-, temperature- and power-dependent photoluminescence (PL) studies. Power dependent PL studies suggests that high-temperature phase (HTP) and low-temperature phase (LTP) can coexist in a wider temperature range depending on the thickness of the 2D perovskite microplates. As the thickness decreases, the structural phase transition temperature first decreases and then increases, in striking contrast to the size dependent phase transition temperature reported previously [6]. By combining the thickness evolution of the emission peaks, the surface depletion field and the surface energy difference between polymorphs are believed to play the dominant role for the anomalous size dependent phase transition here [6, 26-28]. This hypothesis was further supported by the temperature dependent PL studies of the suspended microplates and encapsulated microplates with graphene and hexagonal boron nitride (hBN) flakes. In addition, the surface depletion field induced quantum confinement and Stark effect have also been observed from the thickness and temperature evolution of the PL spectra.

Methods

Sample preparations

(BA)₂PbI₄ bulk crystals were synthesized by a solution method according to previous report [16]. The precursor n-butylammonium iodide (BAI) (2 mmol/mL) was synthesized by dropping a 40% w/w aqueous n-butylamine (4 mL) into a 57% w/w aqueous hydroiodic acid (HI) solution (16 mL) and maintained at 0 °C with strong stirring for 4 h. PbO powder (0.563 g) was dissolved in a mixture of 57% w/w aqueous hydriodic acid (HI) solution (3 mL) and 50% w/w aqueous hypophosphorous acid (H₃PO₂) solution (0.5 mL) by heating to 150 °C under constant magnetic stirring. Then 2.5 mL BAI solution was injected into the resultant solution for synthesis of (BA)₂PbI₄ bulk crystals. Afterwards, the stirring was stopped, and the solution was left to naturally cool to room temperature. The resultant solution was left overnight to complete the growth and the crystals were sequentially isolated by suction filtration and thoroughly dried in the oven.

BAPI microplates were directly exfoliated onto a pre-cleaned 300 nm SiO₂/Si substrate by using the Scotch tape. To cover the microplates with graphene (or hBN), the few-layer graphene (or hBN) flakes were mechanically exfoliated onto the polydimethylsiloxane (PDMS) stamp using the Scotch tape and alignment transferred to the as-exfoliated microplates under the aid of the optical microscope and manipulators. To suspend the BAPI microplates, the holes with a diameter of 10 µm on a 300 nm SiO₂/Si substrate were fabricated by electron beam lithography and inductively coupled plasma etching. Subsequently, BAPI microplates were mechanically exfoliated onto the PDMS stamp and alignment transferred onto the holes under the aid of the optical microscope and manipulators.

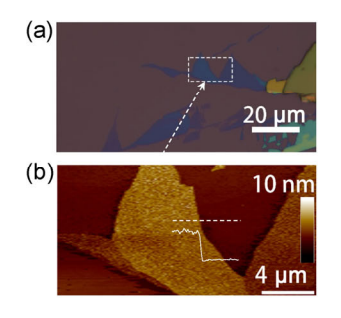
2.2 Material characterizations

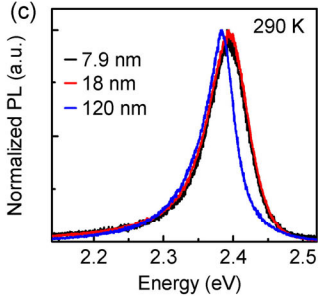
Optical images were acquired on the Olympus BX53M system microscope while the thickness of the perovskite microplates was determined by tapping-mode atomic force microscopy (Bruker Dimension EDGE). The PL spectra were carried out in a confocal micro-Raman system (Horiba HR550) equipped with a 600 g/mm grating in a backscattering configuration excited by a 473-nm solidstate laser. For the low-temperature measurement, we used a liquid nitrogen continuous flow cryostat (Cryo Industry of America, USA) to control the temperature from 78 to 290 K at a base pressure of 10⁻⁶ mBar evacuated by a molecular pump.

Results

BAPI 2D perovskite bulk crystals were synthesized by a solution method as previously reported [16], which undergo an orthorhombicto-orthorhombic transition around 270 K [27]. To investigate how the surface depletion field influences the phase transition, quantum confinement and Stark effect, BAPI microplates with various thicknesses were obtained by mechanical exfoliation method from the bulk crystals using a Scotch tape. The exfoliated microplates with lateral size of micrometers show quite different colors on a 300-nm SiO₂/Si substrate depending on their thicknesses (Fig. 1(a)), which provides a convenient way to identify the thickness of the microplates by their colors, similar to that in graphene and transition metal dichalcogenides [29]. The atomic force microscope (AFM) measurement was carried out to precisely determine the thickness and roughness of the microplates (Fig. 1(b)). AFM images show that the exfoliated microplates undergo quick degradation in ambient. Thus, the asexfoliated microplates were immediately put into the vacuum chamber for further low-temperature PL studies to avoid the degradation.

Figures 1(c) and 1(d) display the normalized PL spectra for three microplates with different thicknesses (7.9, 18 and 120 nm) at 290 and 78 K. While only one broad emission peak with a long tail at the lower energy side was observed at 290 K, PL spectra at 78 K show a rather rich feature, which can be ascribed to self-trapped excitons (STEs), LTP and HTP with multiple emission peaks in each series as indicated in Fig. 1(d) according to previous report [30]. The STEs in 2D perovskites have been widely observed previously due to its smaller formation energy [31-33]. With the increase of the thickness, whereas the emission intensity gradually increases (Fig. S1(a) and S1(b) in the Electronic Supplementary Material (ESM)), the emission peak exhibits an obvious redshift between 120 and 18 nm thick microplates and negligible shift between 18 and 7.9 nm thick microplates due to the surface depletion induced confinement and Stark effect (see





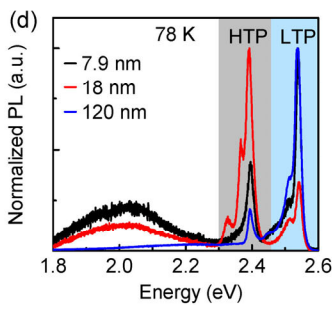


Figure 1 Size dependent PL spectra of BAPI microplates. (a) Optical image of exfoliated BAPI microplates on a 300 nm SiO₂/Si substrate. (b) AFM image for the area highlighted by the white rectangle indicated in (a). The height profile (inset white line) shows a step of 7.9 nm in height at the boundary. (c) and (d) The normalized PL spectra for three perovskite microplates with different thickness at 290 K (c) and 78 K (d).

below and Fig. 1(c)) [26, 34]. At 78 K the intensity of STE peak continuously increases with the reduction of the thickness since the STEs prefer to be localized at the crystallite surfaces and interfaces (Fig. 1(d)) [31]. Interestingly, the intensity ratio of the HTP to LTP increases first and then decreases again with the increase of the thickness (Fig. 1(d)). Similar to 3D perovskite case, the intensity ratio of HTP to LTP can be used to characterize the degree of the structural phase transition in our BAPI microplates [6]. Under a certain temperature, the larger the HTP/LTP ratio is, the lower the structural phase transition temperature is. Thus, we can conclude that the microplate with a thickness of 18 nm has the lowest phase transition temperature among those three microplates, strikingly different from the size dependent phase transition previously reported where the phase transition temperature monotonously decreases with the reduction of the size [9].

In order to verify the coexistence of HTP and LTP, we have carried out temperature- and power-dependent PL studies. Figure 2(a) displays the temperature dependent PL spectra for a 120 nm thick microplate. Two emission bands are clearly observed till 270 K before the phase transition, suggesting the coexistence of those two phases in this temperature range. The full-width at half-maximum (FWHM) extracted from Fig. 2(a) for both LTP and HTP increases with the temperature before phase transition due to the thermal broadening. Importantly, the emission peaks for those two phases show rather different temperature dependence (Figs. 2(b) and 2(c)), confirming the coexistence of two different structural phases. This distinctive temperature dependent emission peak is believed to originate from the different electron–phonon coupling strength and thermal expansion coefficients between those two phases [35, 36].

The power dependent PL spectra at 78 K further verify the coexistence of HTP and LTP and help to assign the multiple emission peaks within those two phase series [37]. Close inspection of the PL spectrum for a 26 nm thick microplate reveals that three emission peaks are present in HTP series and two emission peaks in LTP series (Fig. 2(d)). As the excitation power increases, those peaks maintain at the same positions while the PL intensity linearly increases (Fig. 2(e)), which suggests that those emission peaks are due to either free excitons, self-trapped excitons or phonon replica rather than bound excitons or bi-excitons [38]. Therefore, the peaks at 2.39 and 2.54 eV can be ascribed to the free exciton emission of HTP (X_H) and LTP (X_L) while the relatively broad peaks at 2.33 and 2.52 eV are due to

the self-trapped excitons of HTP (X_{HT}) and LTP (X_{LT}). The peak locating at 2.36 eV might be due to the phonon replica (X_{PR}) within HTP, also supported by the Raman spectrum at 78 K in which a scattering peak at 237 cm⁻¹ was observed, agreeing well with the energy difference between X_{HT} and X_{PR} (Fig. S2 in the ESM) [39]. Those peak assignments were also confirmed by the reflection spectra at 78 K, from which the exciton energies for HTP and LTP were determined to be 2.39 and 2.54 eV respectively, consistent with those in PL spectra (Fig. S3(a) in the ESM). Furthermore, the exciton binding energies for those two phases extracted from reflection spectra are 270 and 470 meV for HTP and LTP respectively, similar to the previous reported values, which further supports our assignments [30, 40].

Similar PL spectra at 78 K were observed for thicker microplates with thicknesses of 105 nm (Fig. 2(f)) and 174 nm (Fig. S3(b) in the ESM) except the relative intensity of peaks which obviously depends on the thickness of microplates. Nevertheless, the emission peaks of HTP show a strikingly different trend with the increase of the excitation power compared with that in the thinner microplates (Fig. 2(d)). While the X_L peak remains at the same energy, the X_H peak shows a gradually blue-shift and the intensity of the X_H peak continuously decreases compared with that of X_L peak for the thicker microplates (Fig. 2(f) and Fig. S3(b) in the ESM). This blue-shift of X_H peak and the reduction of emission intensity of X_H peak in the thicker microplates can be attributed to the band filling effect, which has been observed in quantum dots, quantum wells and CdS nanobelts previously [41, 42]. In the thicker microplates, the structural phase transition is easier, leading to the smaller inclusions of HTP domains within the LTP matrix. Due to the smaller bandgap of HTP, the photogenerated carriers are prone to occupy the small HTP inclusions within LTP, resulting in that a considerable amount of photogenerated carriers are trapped and recombined within the HTP small inclusions (Fig. S4 in the ESM). As the excitation power increases, more and more photogenerated carriers occupy the small HTP inclusions, leading to the quasi-Fermi level of HTP moving into the conduction band and valance band. As a result, the band filling effect takes place, which gives rise to the blue-shift of the emission peak and saturation of the emission intensity [42]. As the thickness decreases, the phase transition becomes much difficult (see below), and thus the size of the HTP inclusions increases resulting in the absence of the band filling effect in the thinner microplates (Fig. 2(d)).

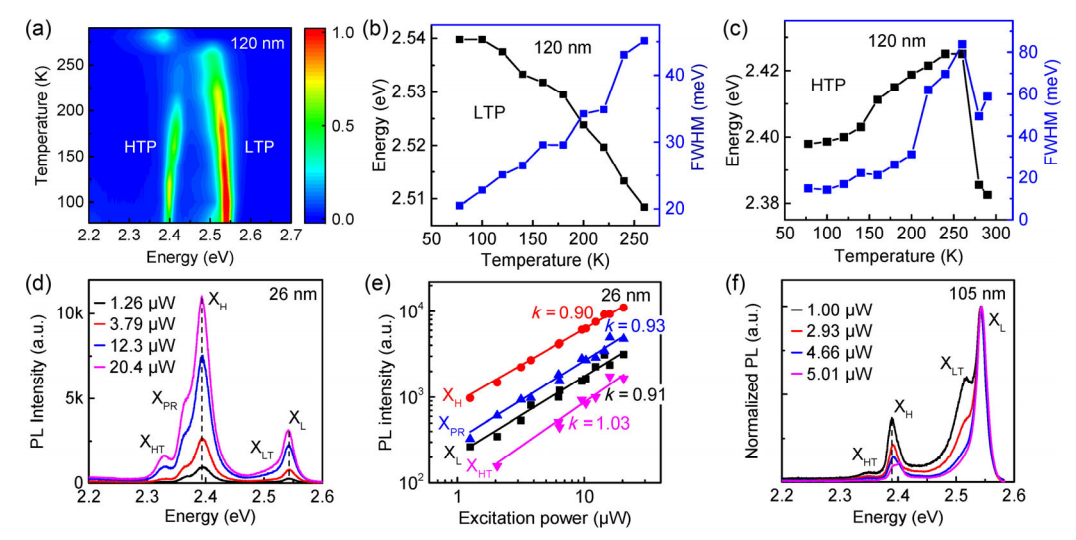


Figure 2 Temperature- and power-dependent PL studies. (a) The temperature dependent PL spectra of a 120-nm thick microplate. (b) and (c) The temperature dependent peak position (black squares) and FWHM (blue squares) of LTP (b) and HTP (c) extracted from (a). (d) The power dependent PL spectra of a 26-nm thick microplate at 78 K under a 473-nm laser excitation. The peak positions of X_L , X_{LT} , X_H , X_{PR} and X_{HT} are 2.54, 2.52, 2.39, 2.36 and 2.33 eV, respectively. (e) The PL intensity versus excitation power extracted from (d). The PL intensity obeys a power-law function of the excitation power ($I_{PL} \sim I_{ex}^k$). The fitting lines give k = 0.91, 0.90, 0.93 and 1.03 for X_L , X_H , X_{PR} and X_{HT} , respectively. (f) Normalized excitation power dependent PL spectra of a 105-nm thick microplate at 78 K under a 473-nm laser excitation.

Therefore, the presence of the band filling effect in the thicker microplates can further support the coexistence of those two phases.

To study the size dependent phase transition in our samples in detail, the temperature dependent PL measurement has been carried out for microplates with various thicknesses. Figures 3(a) and 3(b) display the temperature dependent PL mappings of two typical BAPI microplates with thickness of 7.9 and 26 nm. While LTP dominates the emission at low temperature for the 7.9 nm microplate, the emission is mainly from HTP portion for the 26 nm microplate below 280 K (Figs. 3(a) and 3(b)). The emission energies and FWHMs of X_L and X_H and the intensity ratio of X_L and X_H are extracted from temperature dependent PL spectra for microplates with different thicknesses (Figs. 3(c) and 3(d) and Figs. S5(a)-S5(c) in the ESM). Whereas X_L shows a monotonous red-shift with increasing temperature (Fig. 3(c)), X_H shows a gradual transition from blue-shift to red-shift around the phase transition temperature (Fig. 3(d)). The FWHMs for both X_L and X_H continuously increase with the increase of temperature due to the thermal broadening. Interestingly, the transition temperature of X_H peak strongly depends on the thickness of the microplates and shifts from 270 K for the thicker one above 120 nm to 180 K for the 18 nm thick microplate and then to 220 K again for the thinner one. This trend of the transition temperature with thickness might be closely related to the thickness dependent phase transition, which will be discussed in detail below [30].

Figure 3(e) shows the intensity ratio of HTP to LTP for microplates with various thicknesses from around 5 to 174 nm at 78 K. With the reduction of the thickness, the HTP/LTP ratio first linearly increases till around 30 nm, then shows a sharp increase, subsequently gradually decreases below 25 nm and finally reaches a constant value below 15 nm. As discussed above, the HTP/LTP ratio indicates the degree of the structural phase transition or the phase transition temperature. The thickness dependent structural phase transition above 25 nm agrees well with previous reports [6], which might be attributed to the surface energy differences between those two phases, strain effect or the lack of nucleation sites. In contrast, this trend below 25 nm is rather different from the size dependent phase transition in previously reported material systems [6], where the phase transition temperature monotonously decreases with the geometric size of the nanostructures. The similar trend of the thickness dependent the HTP/LTP ratio has been observed at 140 and 220 K (Figs. S6(a) and S6(b) in the ESM). Therefore, we termed this thickness dependent structural phase transition as anomalous size dependent phase transition due to the strikingly different trend below 25 nm in our samples.

To understand the underlying mechanism for such anomalous size dependent phase transition, we have extracted the thickness evolution of the emission energies for both XH and XL under different temperatures (Figs. 3(f) and 3(g)). At 280 K before phase transition, only one broad peak is present and with the reduction of the thickness the emission peak first blue-shifts and then starts to red-shift with the turning point of 25 nm (Fig. 3(f) and Figs. S7(a) and S7(b) in the ESM). Below 280 K when HTP and LTP coexist, the emission energies for both X_H and X_L almost remain the same for those microplates thicker than 50 nm at all temperatures we investigated (Figs. 3(f) and 3(g)). In contrast, as the thickness decreases below 50 nm, the emission energy of X_H shows a sharp red-shift followed by a blue-shift with the turning point at 25 nm while the emission energy of X_L exhibits a completely opposite trend compared with that of X_H. The turning point of 25 nm agrees excellently with the turning point of the HTP/LTP ratio in Fig. 3(e), which implies that those two behaviors might have the same underlying mechanism. It should be noted that the energy differences between microplates with thickness at the turning point of 25 nm and the very thin (thick) microplates for both X_H and X_L decrease with the lowering temperature (Figs. 3(f) and 3(g)).

The blue-shift of X_H peak with the reduction of thickness at 280 K can be ascribed to the surface depletion induced confinement for the microplates with thickness between 25 and 100 nm and to the reabsorption for the microplates thicker than 100 nm [26]. Since the bulk exciton Bohr radius in BAPI is around 0.55 nm [38], much smaller than 25 nm, we do not anticipate that conventional quantum confinement would be present in our such thick microplates. The blue-shift of X_H emission peak versus $1/L^2$ (where L is the thickness of the microplates) for those microplates thicker than 25 nm indicates that there are two linear regimes with different slopes (Fig. S7(c) in the ESM). According to previous report, the red-shift with increasing thickness for those microplates thicker than 100 nm is resulted from the reabsorption, similar to the case in CdS nanobelts [26]. The emission peak for XH is around 520 nm and the refractive index is around 2 at 520 nm, causing the wavelength of the emission peak within the microplates is estimated to be 260 nm [26]. As a result, the reabsorption would take place for those microplates thicker than

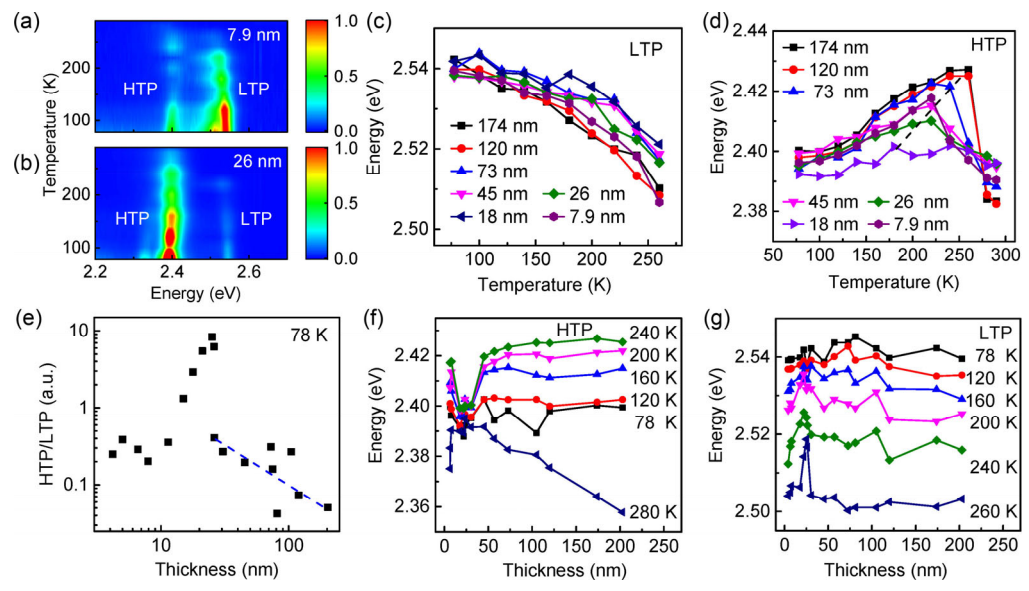


Figure 3 Thickness dependent PL studies. (a) and (b) The temperature dependent PL spectra of the 7.9-nm (a) and 26-nm (b) thick microplate excited by a 473-nm laser with a power of 0.95 μ W. (c) and (d) Temperature dependent peak position of X_L (c) and X_H (d) for microplates with various thicknesses. (e) The thickness dependent HTP/LTP ratio at 78 K. The turning point is around 25 nm. The dashed line is used for guide the eye. (f) and (g) Thickness dependent peak position of X_H (f) and X_L (g) at different temperatures. The turning point is around 25 nm.

130 nm, agreeing well with our observation. For the microplates thinner than 100 nm, the 1/L² dependent X_H emission peak suggests that the surface depletion induced quantum confinement responds to the peak shift [26]. The presence of the surface depletion field would modify the actual potential well to be much smaller than the geometric thickness of the microplate, resulting in the confinement even through the thickness is much larger than the bulk exciton Bohr radius (Fig. S8 in the ESM). For the microplates thinner than 25 nm, the surface depletion field would be even stronger and the red-shift of X_H emission peak with the decrease of the thickness might be due to the quantum confined Stark effect, which is supported by the increase of the FWHMs with reducing the thickness (Fig. S7(d) in the ESM) [43]. When the thickness is larger than 50 nm, the selfabsorption contributes more to the peak broadening. As a result, we observed the jump of FWHM at the thickness of 50 nm. Therefore, we believe the anomalous thickness dependent structural phase transition observed in our samples closely relates to the surface depletion field [44].

Below 280 K after the phase transition occurs, the thickness dependent X_L emission peak follows the same trend as that of the X_H emission peak at 280 K, indicating that the origin for such trend is also the surface depletion induced confinement and quantum confined Stark effect [26]. This hypothesis is further supported by the gradual reduction of the energy difference between microplates with thickness at the turning point of 25 nm and the very thin (thick) microplates as the temperature decreases (Fig. 3(g)). Since the LTP portion dominates over the HTP portion after phase transition, the surface depletion induced electric field mainly distributes inside the LTP portion. As the temperature decreases, the carrier concertation gradually reduces because part of donors or acceptors start to be frozen out. As a result, the surface depletion induced electric field becomes weaker at lower temperature, leading to the weaker confinement and Stark effect and thus the smaller energy difference [45].

In terms of the HTP below the 280 K, this completely opposite trend of X_H emission peak with the thickness can be attributed to the quantum confinement effect [46]. As discussed above, the LTP portion is the dominant phase and the HTP portion is small inclusions embedded within the LTP portion. Thus, the quantum confinement effect would be present in HTP inclusions. As the thickness approaches to the turning point of 25 nm, the HTP portion

increases due to the larger HTP/LTP ratio (Fig. 3(e)), resulting in a relative larger size of the HTP inclusions and thus a weaker quantum confinement effect. As a consequence, the X_H emission peak shows a large red-shift at the turning point. As the temperature decreases, the phase transition continuously processes, leading to the continuously reduction of the HTP portion and thus the size of the small inclusions. Under such case, the size difference of the small inclusions of HTP domains within different thickness microplates gradually decreases, leading to the reduction of the energy difference between microplates with thickness at the turning point of 25 nm and the very thin (thick) microplates (Fig. 3(f)). The surface depletion induced electric field might also play a role in the thickness dependent X_H emission peak shift; nonetheless, it is not the dominant factor [26].

In view of the strong thickness correlation between the emission peak shift for both X_H and X_L and the HTP/LTP ratio with thickness, the surface depletion electric field is believed to be the dominant factor for the anomalous thickness dependent structural phase transition [47]. To verify this hypothesis, we carried out the temperature dependent PL studies for the microplates covered by few-layer graphene flake (semimetal), hBN (insulator) flake or suspended onto holes, by which the surface depletion field would be changed. The microplates are only partially covered or suspended so that we can easily compare how the PL spectrum changes after the samples are covered or suspended. To exclude that the change of PL spectra between the covered and uncovered portion is not from the degradation of the microplates themselves, we have acquired PL spectra of the same microplates at 290 K before and after the low temperature PL measurement, from which no noticeable change was observed (Fig. S9 in the ESM). This suggests that the microplates would not undergo substantial degradation during the measurement period and the spectral difference between the uncovered (unsuspended) and covered (suspended) portion should not be attributed to the degradation of the samples.

While the HTP/LTP ratio is significantly reduced after covered by either graphene or hBN flakes, suspended on hole would in contrast increase the HTP/LTP ratio, suggesting that the phase transition would be enhanced in covered microplates and suppressed in suspended samples (Fig. 4). In addition, the emission from self-trapped states X_T is greatly suppressed and the emission intensities of X_H and X_L are significantly enhanced after the microplates are covered by either graphene or hBN with a much bigger enhancement

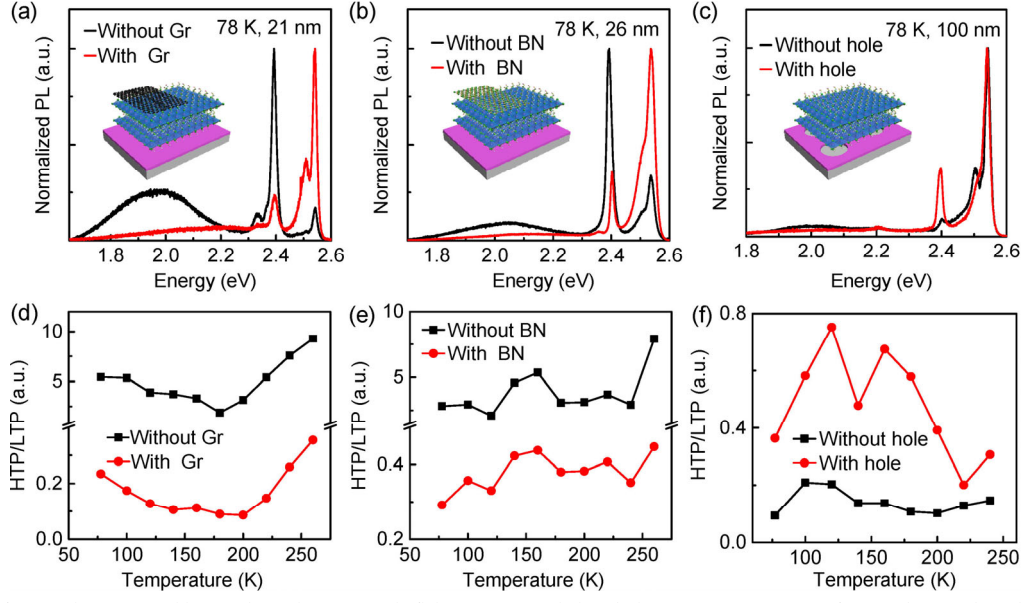


Figure 4 PL spectra of microplates covered by graphene, boron nitride flakes, or suspended on holes. (a)–(c) PL spectra of microplates with/without graphene (a), boron nitride (b) and suspended on holes (c) at 78 K. The diameter of the hole is 10 µm. The insets of (a)–(c) show the schematic diagrams of device structure. (d)–(f) The temperature dependent HTP/LTP ratio for microplates with/without graphene (d), boron nitride (e) and suspended on holes (f).

6 Nano Res.

for graphene covered microplates (Figs. 4(a) and 4(b) and Figs. S10(a) and S10(b) in the ESM). In contrast, PL is quenched after the microplate is suspended on holes (Fig. S10(c) in the ESM). The similar PL intensity change has been also observed at room temperature for all those covered and suspended samples (Figs. S10(d)-S10(f) in the ESM). While the suppression of X_T emission might be due to the surface passivation which reduces the extrinsic self-trapped states, the enhanced PL intensity for the covered samples with both semimetal graphene and insulator hBN reveals that the surface depletion electric field would be reduced for the covered samples, leading to the reduction of the exciton ionization induced by electric field. As a result, the PL intensities for both X_{H} and X_{L} are enhanced. The semimetal graphene layer would more favor the charge transfer compared with insulator hBN, thus giving rise to a much larger reduction of the surface depletion field and much larger enhanced PL intensities for both X_H and X_L in the graphene covered microplates. Furthermore, the FWHMs become narrower for the covered samples due to the reduced field broadening, which also supports that the surface depletion field is reduced for the covered samples (Fig. S11 in the ESM). Besides, we observed the emission peak position shift in PL spectra for the covered and suspended microplates, which may be able to be ascribed to the macroscopic strain [48]. For the suspended microplates, both sides of the microplates are exposed in air, which would increase the surface depletion field either due to introducing more surface states or due to the change of the surrounding dielectric environment. Consequently, the exciton ionization is more severe resulting in the quench of the PL emission for the suspended samples (Figs. 4(c) and 4(f)). To sum up, all those experimental evidences again support that the surface depletion electric field is responsible for the anomalous size dependent phase transition [49].

We also carried out the thickness dependent PL studies for the covered and suspended microplates to further identify that the surface depletion field indeed plays a dominant role in the anomalous size dependent phase transition in our samples. Figure 5 displays the HTP/LTP ratio for the covered and suspended microplates with various thicknesses at 78 K. After covering with either graphene or hBN, the HTP/LTP ratio decreases to a similar value for all thicknesses, suggesting that the surface depletion field is reduced to such a level that all samples behave as the very thick microplates and thus the phase transition is enhanced to the same level for all samples. In contrast, the decrease of the HTP/LTP ratio clearly reveals the slight suppression of the phase transition in the suspended samples although only a slight change of emission peak and FWHMs is observed, which is due to the relatively thick microplates (~ 100 nm) we used. Those results further strengthen the conclusion we achieved above that the surface depletion electric field is the main reason responsible for the anomalous size dependent phase transition.

4 Discussion

The presence of the large surface depletion field in our samples is unexpected since the van der Waals coupling among layers in 2D perovskites would be free of the surface dangling bonds and thus the surface states, similar to graphene and other layered materials [50]. Nevertheless, our experimental results indicate that a considerable amount of surface states are present in our BAPI microplates, supported by the thickness and temperature dependent PL studies of uncovered, covered and suspended microplates. One possible reason for the presence of the surface states is the surface reconstruction induced by the accumulation of the elastic energy near the surfaces [51]. As a result, the lower energy electronic states are formed near the surfaces, leading to the surface depletion field. Alternatively, the perfect crystal lattices near surfaces have been

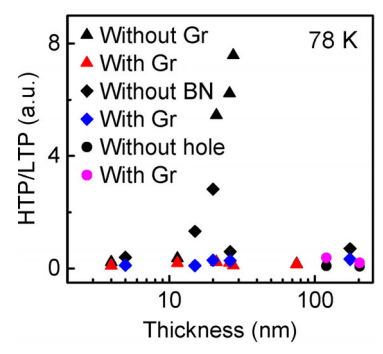


Figure 5 The thickness dependent HTP/LTP ratio for microplates with/without graphene, and boron nitride and suspended on holes at 78 K.

broken during the sample preparation process supported by the rather rough surface for the exfoliated microplates (Fig. 1(b)). Consequently, the surface states are formed leading to the formation of the surface depletion field. In our case, it seems both of them are responsible for the observed strong surface depletion field.

The electric field enhanced phase transition in our samples might originate from the electric field induced strain, which alters the interfacial energy leading to the change of the phase transition temperature. During the structural phase transition process of a crystal, crystal lattice distortion will occur, resulting in strain [52]. How the internal stress affects the structural phase transition temperature has been reported previously and we believe it is also responsible for the size dependent structural phase transition observed in our experiments [53-55]. The growth of the phase domains depends on the competition between the bulk energy of each phase and interfacial energy between those two associated phases [6]. The phase domains are prone to grow if the bulk energy of the phase decreases while the domains favor shrinkage when the interfacial energy between those two phases increases. Thus, the growth of the phase domains becomes energetically unfavorable if the size of phase domains is smaller than a critical size. Previous studies reveal that BAPI 2D perovskites exhibit ferroelectricity and thus the surface depletion electric field would create strain within BAPI microplates [42, 56]. The electric field induced strain would modify the interfacial energy and thus increase the critical size of the HTP phase. Some of the HTP inclusions are smaller than the critical size, leading to the shrinkage of the HTP domains. As a result, the HTP/LTP ratio reduces for the very thinner microplates. Nevertheless, further investigations are required to clarify this field enhanced phase transition.

5 Conclusion

In summary, we have systematically investigated how the surface depletion field affects the structural phase transition, quantum confinement and Stark effect in 2D (BA)₂PbI₄ perovskite microplates by the thickness-, temperature- and power-dependent PL studies. The thickness dependent phase transition for microplates thinner than 25 nm is strikingly different from that in other nanomaterial systems. By combining the thickness dependent emission energy and PL spectra of covered and suspended microplates, the anomalous thickness dependent phase transition might be attributed to the surface depletion electric field, which changes the interfacial energy between those two phases and thus the critical size of HTP. In addition, the surface depletion field induced quantum confinement and Stark effect take place, which manifest themselves by the thickness- and temperature-dependent free excition emission peaks. The size dependent phase transition would affect the performance of optoelectronic devices operating at low temperature or in airplanes and satellites. Thus, our studies could provide insight how to properly control the size of the samples to achieve the optimal performance for the optoelectronic devices. In addition, the coexistence of two phases allows us to realize dual color light emission and detection by properly designing the size of samples, which would find important applications in optical imaging.

Acknowledgements

D. H. L. acknowledges support from the National Natural Science Foundation of China (No. 61674060), Innovation Fund of WNLO and the Fundamental Research Funds for the Central Universities, HUST (Nos. 2017KFYXJJ030, 2017KFXKJC003, 2017KFXKJC002, and 2018KFYXKJC016); H. M. L. is grateful for support from New Mexico EPSCoR with NSF-1301346. We thank Testing Center of Huazhong University of Science and Technology for the support in inductively coupled plasma etching.

Electronic Supplementary Material: Supplementary material (spplementary figures) is available in the online version of this article at https://doi.org/10.1007/s12274-019-2524-3.

References

- [1] Leng, K.; Abdelwahab, I.; Verzhbitskiy, I.; Telychko, M.; Chu, L. Q.; Fu, W.; Chi, X.; Guo, N.; Chen, Z. H.; Chen, Z. X. et al. Molecularly thin two-dimensional hybrid perovskites with tunable optoelectronic properties due to reversible surface relaxation. *Nat. Mater.* 2018, 17, 908–914.
- [2] Gerosa, M.; Gygi, F.; Govoni, M.; Galli, G. The role of defects and excess surface charges at finite temperature for optimizing oxide photoabsorbers. *Nat. Mater.* 2018, 17, 1122–1127.
- [3] Long, G. K.; Zhou, Y. C.; Zhang, M. T.; Sabatini, R.; Rasmita, A.; Huang, L.; Lakhwani, G.; Gao, W. B. Theoretical prediction of chiral 3D hybrid organic–inorganic perovskites. *Adv. Mater.* 2019, 31, 1807628.
- [4] Chen, Y. N.; Sun, Y.; Peng, J. J.; Tang, J. H.; Zheng, K. B.; Liang, Z. Q. 2D Ruddlesden-Popper perovskites for optoelectronics. Adv. Mater. 2018, 30, 1703487.
- [5] Qi, X.; Zhang, Y. P.; Ou, Q. D.; Ha, S. T.; Qiu, C. W.; Zhang, H.; Cheng, Y. B.; Xiong, Q. H.; Bao, Q. L. Photonics and optoelectronics of 2D metal-halide perovskites. *Small* 2018, 14, 1800682.
- [6] Li, D. H.; Wang, G. M.; Cheng, H. C.; Chen, C. Y.; Wu, H.; Liu, Y.; Huang, Y.; Duan, X. F. Size-dependent phase transition in methylammonium lead iodide perovskite microplate crystals. *Nat. Commun.* 2016, 7, 11330.
- [7] Xi, X. X.; Wang, Z. F.; Zhao, W. W.; Park, J. H.; Law, K. T.; Berger, H.; Forró, L.; Shan, J.; Mak, K. F. Ising pairing in superconducting NbSe₂ atomic layers. *Nat. Phys.* 2016, 12, 139–143.
- [8] Xi, X. X.; Zhao, L.; Wang, Z. F.; Berger, H.; Forró, L.; Shan, J.; Mak, K. F. Strongly enhanced charge-density-wave order in monolayer NbSe₂. Nat. Nanotechnol. 2015, 10, 765–769.
- [9] Yu, Y. J.; Yang, F. Y.; Lu, X. F.; Yan, Y. J.; Cho, Y. H.; Ma, L. G.; Niu, X. H.; Kim, S.; Son, Y. W.; Feng, D. L. et al. Gate-tunable phase transitions in thin flakes of 1T-TaS₂. Nat. Nanotechnol. 2015, 10, 270–276.
- [10] Wang, Z. Y.; Sun, Y. Y.; Abdelwahab, I.; Cao, L.; Yu, W.; Ju, H. X.; Zhu, J. F.; Fu, W.; Chu, L. Q.; Xu, H. et al. Surface-limited superconducting phase transition on 1T-TaS₂. ACS Nano 2018, 18, 1936–0851.
- [11] Chen, L.; Liu, J.; Jiang, C.; Zhao, K. P.; Chen, H. Y.; Shi, X.; Chen, L. D.; Sun, C. H.; Zhang, S. B.; Wang, Y. et al. Nanoscale behavior and manipulation of the phase transition in single-crystal Cu₂Se. Adv. Mater. 2019, 31, 1804919.
- [12] Kang, Y. M.; Najmaei, S.; Liu, Z.; Bao, Y. J.; Wang, Y. M.; Zhu, X.; Halas, N. J.; Nordlander, P.; Ajayan, P. M.; Lou, J. et al. Plasmonic hot electron induced structural phase transition in a MoS₂ monolayer. *Adv. Mater.* 2014, 26, 6467–6471.
- [13] Bai, S.; Wu, Z. W.; Wu, X. J.; Jin, Y. Z.; Zhao, N.; Chen, Z. H.; Mei, Q. Q.; Wang, X.; Ye, Z. Z.; Song, T. et al. High-performance planar heterojunction perovskite solar cells: Preserving long charge carrier diffusion lengths and interfacial engineering. *Nano Res.* 2014, 7, 1749–1758.
- [14] Miyata, A.; Mitioglu, A.; Plochocka, P.; Portugall, O.; Wang, J. T. W.; Stranks, S. D.; Snaith, H. J.; Nicholas, R. J. Direct measurement of the exciton binding energy and effective masses for charge carriers in organic-inorganic tri-halide perovskites. *Nat. Phys.* 2015, 11, 582–587.

- [15] Li, L.; Li, J. Z.; Lan, S. G.; Lin, G. M.; Wang, J.; Wang, H. Z.; Xuan, Y. N.; Luo, H. M.; Li, D. H. Two-step growth of 2D organic-inorganic perovskite microplates and arrays for functional optoelectronics. *J. Phys. Chem. Lett.* 2018, 9, 4532–4538.
- [16] Stoumpos, C. C.; Cao, D. H.; Clark, D. J.; Young, J.; Rondinelli, J. M.; Jang, J. I.; Hupp, J. T.; Kanatzidis, M. G. Ruddlesden–Popper hybrid lead iodide perovskite 2D homologous semiconductors. *Chem. Mater.* 2016, 28, 2852–2867.
- [17] Wang, J.; Li, J. Z.; Tan, Q. H.; Li, L.; Zhang, J. B.; Zang, J. F.; Tan, P. H.; Zhang, J.; Li, D. H. Controllable synthesis of two-dimensional ruddlesdenpopper-type perovskite heterostructures. *J. Phys. Chem. Lett.* 2017, 8, 6211–6219.
- [18] Yan, F.; Xing, J.; Xing, G. C.; Quan, L.; Tan, S. T.; Zhao, J. X.; Su, R.; Zhang, L. L.; Chen, S.; Zhao, Y. W. et al. Highly efficient visible colloidal lead-halide perovskite nanocrystal light-emitting diodes. *Nano Lett.* 2018, 18, 3157–3164.
- [19] Li, X. M.; Wu, Y.; Zhang, S. L.; Cai, B.; Gu, Y.; Song, J. Z.; Zeng, H. B. CsPbX₃ quantum dots for lighting and displays: Room-temperature synthesis, photoluminescence superiorities, underlying origins and white light-emitting diodes. *Adv. Funct. Mater.* 2016, 26, 2435–2445.
- [20] Lin, K. B.; Xing, J.; Quan, L. N.; de Arquer, F. P. G.; Gong, X. W.; Lu, J. X.; Xie, L. Q.; Zhao, W. J.; Zhang, D.; Yan, C. Z. et al. Perovskite light-emitting diodes with external quantum efficiency exceeding 20 per cent. *Nature* 2018, 562, 245–248.
- [21] Wang, J.; Su, R.; Xing, J.; Bao, D.; Diederichs, C.; Liu, S.; Liew, T. C. H.; Chen, Z. H.; Xiong, Q. H. Room temperature coherently coupled exciton– polaritons in two-dimensional organic–inorganic perovskite. ACS nano 2018, 12, 8382–8389.
- [22] Fang, Y. J.; Dong, Q. F.; Shao, Y. H.; Yuan, Y. B.; Huang, J. S. Highly narrowband perovskite single-crystal photodetectors enabled by surfacecharge recombination. *Nat. Photonics* 2015, 9, 679–686.
- [23] Di, J.; Xiong, J.; Li, H. M.; Liu, Z. Ultrathin 2D photocatalysts: Electronic-structure tailoring, hybridization, and applications. Adv. Mater. 2018, 30, 1704548.
- [24] Zhu, C.; Chen, Y.; Liu, F. C.; Zheng, S. J.; Li, X. B.; Chaturvedi, A.; Zhou, J. D.; Fu, Q. D.; He, Y. M.; Zeng, Q. S. et al. Light-tunable 1T-TaS₂ charge-density-wave oscillators. ACS Nano 2018, 12, 11203–11210.
- [25] Long, G. K.; Jiang, C. Y.; Sabatini, R.; Yang, Z. Y.; Wei, M. Y.; Quan, L. N.; Liang, Q. M.; Rasmita, A.; Askerka, M.; Walters, G. et al. Spin control in reduced-dimensional chiral perovskites. *Nat. Photonics* 2018, 12, 528–533.
- [26] Li, D. H.; Zhang, J.; Xiong, Q. H. Surface depletion induced quantum confinement in CdS nanobelts. ACS Nano 2012, 6, 5283–5290.
- [27] Billing, D. G.; Lemmerer, A. Synthesis, characterization and phase transitions in the inorganic-organic layered perovskite-type hybrids $[(C_nH_{2n+1}NH_3)_2PbI_4]$, n = 4, 5 and 6. *Acta Crystallogr., Sect. B: Struct. Sci.* **2007**, *63*, 735–747.
- [28] Lai, M. L.; Kong, Q.; Bischak, C. G.; Yu, Y.; Dou, L.; Eaton, S. W.; Ginsberg, N. S.; Yang, P. D. Structural, optical, and electrical properties of phase-controlled cesium lead iodide nanowires. *Nano Res.* 2017, 10, 1107–1114.
- [29] Li, J. Z.; Wang, J.; Zhang, Y. J.; Wang, H. Z.; Lin, G. M.; Xiong, X.; Zhou, W. H; Luo, H. M.; Li, D. H. Fabrication of single phase 2D homologous perovskite microplates by mechanical exfoliation. 2D Mater. 2018, 5, 021001.
- [30] Yaffe, O.; Chernikov, A.; Norman, Z. M.; Zhong, Y.; Velauthapillai, A.; van der Zande, A.; Owen, J. S.; Heinz, T. F. Excitons in ultrathin organic-inorganic perovskite crystals. *Phys. Rev. B* 2015, 414.
- [31] Wu, X. X.; Trinh, M. T.; Niesner, D.; Zhu, H. M.; Norman, Z.; Owen, J. S.; Yaffe, O.; Kudisch, B. J.; Zhu, X. Y. Trap states in lead iodide perovskites. J. Am. Chem. Soc. 2015, 137, 2089–2096.
- [32] Thirumal, K.; Chong, W. K.; Xie, W.; Ganguly, R.; Muduli, S. K.; Sherburne, M.; Asta, M.; Mhaisalkar, S.; Sum, T. C.; Soo, H. S. et al. Morphology-independent stable white-light emission from self-assembled two-dimensional perovskites driven by strong exciton-phonon coupling to the organic framework. *Chem. Mater.* 2017, 29, 3947–3953.
- [33] Li, J. Z.; Wang, J.; Ma, J. Q.; Shen, H. Z.; Li, L.; Duan, X. F.; Li, D. H. Self-trapped state enabled filterless narrowband photodetections in 2D layered perovskite single crystals. *Nat. Commun.* 2019, 10, 806.
- [34] Li, D. H.; Zhang, J.; Zhang, Q.; Xiong, Q. H. Electric-field-dependent photoconductivity in CdS nanowires and nanobelts: Exciton ionization, Franz–Keldysh, and Stark effects. *Nano Lett.* 2012, 12, 2993–2999.
- [35] Gauthron, K.; Lauret, J. S.; Doyennette, L.; Lanty, G.; Al Choueiry, A.; Zhang, S. J.; Brehier, A.; Largeau, L.; Mauguin, O.; Bloch, J. et al. Optical

Nano Res.

spectroscopy of two-dimensional layered $(C_6H_5C_2H_4-NH_3)_2-PbI_4$ perovskite. *Opt. Express* **2010**, *18*, 5912–5919.

- [36] Chen, Z. Z.; Wang, Y. P.; Sun, X.; Xiang, Y.; Hu, Y.; Jiang, J.; Feng, J.; Sun, Y. Y.; Wang, X.; Wang, G. C. et al. Remote phononic effects in epitaxial Ruddlesden-Popper halide perovskites. J. Phys. Chem. Lett. 2018, 9, 6676–6682.
- [37] Gan, L.; Li, J.; Fang, Z. S.; He, H. P.; Ye, Z. Z. Effects of organic cation length on exciton recombination in two-dimensional layered lead iodide hybrid perovskite crystals. J. Phys. Chem. Lett. 2017, 8, 5177–5183.
- [38] Blancon, J. C.; Stier, A. V.; Tsai, H.; Nie, W.; Stoumpos, C. C.; Traoré, B.; Pedesseau, L.; Kepenekian, M.; Katsutani, F.; Noe, G. T. et al. Scaling law for excitons in 2D perovskite quantum wells. *Nat. Commun.* 2018, 9, 2254.
- [39] Ni, L. M.; Huynh, U.; Cheminal, A.; Thomas, T. H.; Shivanna, R.; Hinrichsen, T. F.; Ahmad, S.; Sadhanala, A.; Rao, A. Real-time observation of exciton-phonon coupling dynamics in self-assembled hybrid perovskite quantum wells. ACS Nano 2017, 11, 10834–10843.
- [40] Zhang, Q.; Chu, L. Q.; Zhou, F.; Ji, W.; Eda, G. Excitonic properties of chemically synthesized 2D organic-inorganic hybrid perovskite nanosheets. *Adv. Mater.* 2018, 30, 1704055.
- [41] Manser, J. S.; Kamat, P. V. Band filling with free charge carriers in organometal halide perovskites. *Nat. Photonics* 2014, 8, 737–743.
- [42] Li, D. H.; Liu, Y.; de la Mata, M.; Magen, C.; Arbiol, J.; Feng, Y. P.; Xiong, Q. H. Strain-induced spatially indirect exciton recombination in zinc-blende/wurtzite CdS heterostructures. *Nano Res.* 2015, 8, 3035–3044.
- [43] Walters, G.; Wei, M.; Voznyy, O.; Quintero-Bermudez, R.; Kiani, A.; Smilgies, D. M.; Munir, R.; Amassian, A.; Hoogland, S.; Sargent, E. The quantum-confined Stark effect in layered hybrid perovskites mediated by orientational polarizability of confined dipoles. *Nat. Commun.* 2018, 9, 4214.
- [44] Zhao, F. H.; Gao, X.; Fang, X.; Glinka, Y. D.; Feng, X. Y.; He, Z. B.; Wei, Z. P.; Chen, R. Interfacial-field-induced increase of the structural phase transition temperature in organic-inorganic perovskite crystals coated with ZnO nanoshell. *Adv. Mater. Interfaces* 2018, 5, 1800301.
- [45] Roch, J. G.; Leisgang, N.; Froehlicher, G.; Makk, P.; Watanabe, K.; Taniguchi, T.; Schönenberger, C.; Warburton, R. J. Quantum-confined stark effect in a MoS₂ monolayer van der waals heterostructure. *Nano Lett.* 2018, 18, 1070–1074.

- [46] Sichert, J. A.; Tong, Y.; Mutz, N.; Vollmer, M.; Fischer, S.; Milowska, K. Z.; García Cortadella, R.; Nickel, B.; Cardenas-Daw, C.; Stolarczyk, J. K. et al. Quantum size effect in organometal halide perovskite nanoplatelets. *Nano Lett.* 2015, 15, 6521–6527.
- [47] Hapuarachchi, H.; Gunapala, S. D.; Bao, Q. L.; Stockman, M. I.; Premaratne, M. Exciton behavior under the influence of metal nanoparticle near fields: Significance of nonlocal effects. *Phys. Rev. B* 2018, 98, 115430.
- [48] Tu, Q.; Spanopoulos, I.; Hao, S. Q.; Wolverton, C.; Kanatzidis, M. G.; Shekhawat, G. S.; Dravid, V. P. Probing strain-induced band gap modulation in 2D hybrid organic-inorganic perovskites. ACS Energy Lett. 2019, 4, 796–802
- [49] Kepenekian, M.; Traore, B.; Blancon, J. C.; Pedesseau, L.; Tsai, H.; Nie, W.; Stoumpos, C. C.; Kanatzidis, M. G.; Even, J.; Mohite, A. D. et al. Concept of lattice mismatch and emergence of surface states in two-dimensional hybrid perovskite quantum wells. *Nano Lett.* 2018, 18, 5603–5609.
- [50] Liu, Y.; Guo, J.; Zhu, E. B.; Liao, L.; Lee, S. J.; Ding, M. N.; Shakir, I.; Gambin, V.; Huang, Y.; Duan, X. F. Approaching the Schottky–Mott limit in van der Waals metal–semiconductor junctions. *Nature* 2018, 557, 696–700.
- [51] Zhang, K. Q.; Liu, X. Y. In situ observation of colloidal monolayer nucleation driven by an alternating electric field. Nature 2004, 429, 739–743.
- [52] Jin, F.; Ji, J. T.; Xie, C.; Wang, Y. M.; He, S. N.; Zhang, L.; Yang, Z. R.; Yan, F.; Zhang, Q. M. Characterization of structural transitions and lattice dynamics of hybrid organic–inorganic perovskite CH₃NH₃PbI₃. *Chin. Phys. B.* 2019, 28, 076102.
- [53] Zeches, R. J.; Rossell, M. D.; Zhang, J. X.; Hatt, A. J.; He, Q.; Yang, C. H.; Kumar, A.; Wang, C. H.; Melville, A.; Adamo, C. et al. A strain-driven morphotropic phase boundary in BiFeO₃. Science 2009, 326, 977–980.
- [54] Wehrenfennig, C.; Liu, M. Z.; Snaith, H. J.; Johnston, M. B.; Herz, L. M. Charge carrier recombination channels in the low-temperature phase of organic-inorganic lead halide perovskite thin films. APL Mater. 2014, 2, 081513.
- [55] Hatt, A. J.; Spaldin, N. A.; Ederer, C. Strain-induced isosymmetric phase transition in BiFeO₃. Phys. Rev. B 2010, 81, 054109.
- [56] You, Y. M.; Liao, W. Q.; Zhao, D. W.; Ye, H. Y.; Zhang, Y.; Zhou, Q. H.; Niu, X. H.; Wang, J. L.; Li, P. F.; Fu, D. W. et al. An organic-inorganic perovskite ferroelectric with large piezoelectric response. *Science* 2017, 357, 306–309.